ELSEVIER

Journal of Electron Spectroscopy and Related Phenomena 88–91 (1998) 59–64

JOURNAL OF ELECTRON SPECTROSCOPY and Related Phenomena

Dichroism in (e,2e) ionizing collisions with laser-oriented sodium atoms

J. Berakdar*, A. Dorn[1], A. Elliott, J. Lower, E. Weigold

Atomic and Molecular Physics Laboratories, Research School of Physical Sciences and Engineering, Institute of Advanced Studies, Australian National University, Canberra ACT 0200, Australia

Abstract

The first experimental observation of 'orientational dichroism' in electron impact-induced ionization is discussed. (e,2e) experiments on pure angular momentum states of sodium, excited by right- and left-handed circularly polarized laser light, show that the angular distributions of the final state electron pair are strongly dependent on initial state orientation of the target. Comparison with calculation demonstrates the dependence of the dichroism on details of the scattering dynamics. © 1998 Elsevier Science B.V.

Keywords: Ionization; (e,2e) collisions; Laser excitation; Sodium; PACS NUMBERS: 34.80Dp

1. Introduction

In the (e,2e) technique [1–3], an incident electron beam of well defined energy and direction (momentum) impinges on a chosen gaseous or solid target. Pairs of electrons from single collision events are identified, after energy and momentum analysis, by their arrival in time coincidence at two separate detectors. Depending upon the reaction kinematics selected, the experiment can be used to highlight detailed information on the collision dynamics [1,2] or be used as a sensitive spectroscopic probe to reveal electron momentum distributions in isolated atoms and molecules [2,3] or in condensed matter [4].

We report here on (e,2e) experiments in which additionally the projection quantum number for an excited atomic target in a pure non-zero angular momentum state is resolved. An atomic sodium target is laser excited to the $3^2P_{3/2}F = 3, m_F = +3$ or $m_F = -3$ hyperfine states, consisting of maximal projections of the nuclear spin ($m_I = \pm 3/2$), the orbital angular momentum ($m_L = \pm 1$) and the electron spin ($m_S = \pm 1/2$) along the laser beam direction.

Fig. 1 shows schematically the co-planar asymmetric scattering geometry employed in the present work, in which the momentum vectors $\mathbf{p}_0$, $\mathbf{p}_a$ and $\mathbf{p}_b$ of the incident and two final state continuum electrons of respective energies E_0, E_a and E_b are confined to a common plane. Also shown schematically in the figure are the charge density distributions for the $m_L = 0$ (unoccupied) and $m_L = \pm 1$ excited states of sodium. The experiments consisted of measuring the (e,2e) ionization cross-section for a fixed scattering angle θ_a of the fast emitted electron as a function of the scattering angle θ_b for the slow electron and for both positive ($m_L = +1$) and negative ($m_L = -1$) orbital

* Author to whom correspondence should de addressed. Present address: Max-Planck Institute for Microstructure Physics, Weinberg 2, 06120 Halle, Germany.

[1] Present address: Fakultät für Physik, Albert–Ludwigs-Universität, Hermann–Herder–Strasse 3, 79104 Freiburg, Germany.

PII S0368-2048(97)00117-5

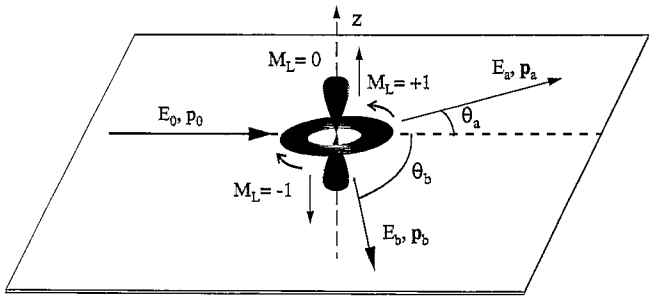

Fig. 1. Schematic representation of the (e,2e) reaction kinematics showing momentum vectors $\vec{p}_0$, $\vec{p}_a$ and $\vec{p}_b$ and respective energies E_0, E_a, and E_b of the incident and two final state continuum electrons, the charge clouds associated with the excited $3p$ sodium orbitals and the orientation of the $m_L = \pm 1$ states with respect to the quantization axis z, which coincides with the laser beam direction.

orientations of the excited state. This figure shows that experiments with positive and negative orbital angular momentum orientation are distinguishable from one another and therefore may give rise to different cross-sections, as reflection of the reaction kinematics in the plane perpendicular to the reaction plane and parallel to the incident beam direction, whilst reversing the sense of orbital orientation, also interchanges the two momentum vectors associated with the two outgoing electrons. Thus the collision system possesses a chirality defined by the orientation of an achiral atomic orbital with respect to the scattering plane.

These basic symmetry arguments point to the possibility of a difference in the ionization cross-section for positively and negatively orientated orbitals i.e. an 'orientational dichroism'. Indeed, the calculations of Fehr, Berakdar and Klar [5] predicted a finite magnitude orientational dichroism for the ionization of oriented H $2p$. The underlying mechanism was found to be the transfer of atomic target orientation to the final state continuum electron pair. Our experimental results, described later, constitute the first experimental observation of this effect in electron impact ionization.

2. Experimental

The main features of our (e,2e) apparatus were described in detail previously [6]. A beam of unpolarized electrons is produced by photo-emission from a negative electron affinity GaAs crystal surface illuminated by linearly polarized infra-red laser radiation. The target beam of sodium atoms required for the present measurements is produced by effusion of sodium gas through a 1 mm aperture positioned at the output stage of a recirculating oven. Intersecting at right angles the plane defined by the electron and sodium beams and the emitted electrons, and completely encompassing the region formed by their overlap, is a 589 nm laser beam used to excite the sodium atoms (Fig. 1). The initially linearly polarized laser light is converted to circularly polarized radiation by transmission through a quarter wave plate, the rotation of which by 90° reverses the helicity of the radiation field and hence the sign of the laser induced target orientation.

Excitation of the atomic sodium is achieved by means of two laser frequencies produced by frequency modulation of a single mode dye-laser beam using an electro–optical modulator. One frequency is tuned to the transition $3S_{1/2}(F=2) \rightarrow 3P_{3/2}(F=3)$, the other to the transition $3S_{1/2}(F=1) \rightarrow 3P_{3/2}(F=2)$. In this way a relative fraction of about 40% $3P_{3/2}$ states is reached [7]. After a few excitation/decay cycles the atoms gather exclusively in the two level systems $3S_{1/2}(F=2, m_F=+2) \leftrightarrow 3P_{3/2}(F=3, m_F=+3)$ for pumping by σ^+ radiation and $3S_{1/2}(F=2, m_F=-2) \leftrightarrow 3P_{3/2}(F=3, m_F=-3)$ for pumping by σ^-, respectively, resulting in a degree of excited state orientation of between 96% and 100%. Pairs of emitted electrons are detected in time coincidence in two separate rotatable hemispherical electrostatic electron analysers. The analysers [6] incorporate position sensitive detectors, enabling simultaneous measurement over a 6 eV

energy band with a resolution of around 0.2 eV, leading to a total coincidence (e,2e) resolution of around 0.9 eV.

3. Theory

The (e,2e) cross-section is irreducibly described by a set of tensorial parameters whose number is determined by the symmetry of the initially prepared target state [8], and for a target with total angular momentum J it can be written as

$$\frac{d^5\sigma}{d\Omega_a d\Omega_b dE_b} = \sum_{i=0}^{2J} \rho_{i0}\Lambda_0^{(i)} \tag{1}$$

where the tensorial components $\Lambda_0^{(i)}$ along the quantization axis of the target describe the dynamics of the ionization process, and ρ_{i0} are the state multipoles describing the M-state population of the target. The transformation properties of $\Lambda_0^{(i)}$ are determined by the rank i of the associated tensor. In the present case of the Na $3P_{3/2}$ state it suffices to consider Eq. (1) with respect to only the orbital angular momentum $L = 1$ for singlet and triplet scattering. Then the cross-section is described by only three tensorial components $\Lambda_0^{(i)}$, which can be written in terms of the ionization cross-sections for the individual magnetic substates σ_{L,m_L}:

$$\Lambda_0^{(0)} = \frac{1}{\sqrt{3}}(\sigma_{1,1} + \sigma_{1,0} + \sigma_{1,-1}) \tag{2}$$

$$\Lambda_0^{(1)} = \frac{1}{\sqrt{2}}(\sigma_{1,1} - \sigma_{1,-1}) \tag{3}$$

$$\Lambda_0^{(2)} = \frac{1}{\sqrt{6}}(\sigma_{1,1} - 2\sigma_{1,0} + \sigma_{1,-1}) \tag{4}$$

The scalar component $\Lambda_0^{(0)}$ yields the averaged TDCS for statistically populated m_L states, while the deviation of this cross-section from that for the ionization of the $m_L = 0$ state is indicated by the alignment component $\Lambda_0^{(2)}$. The quantity $\Lambda_0^{(1)}$ is a vector component and is a measure of the change in the cross-section resulting from an inversion of the initial target orientation. We measure all of the parameters in eqns (2)–(4) as $\sigma_{1,0}$ is zero in the present experimental arrangement (Fig. 1). The cross-sections σ_{L,m_L} are given by

$$\sigma_{L,m_L} = C|T_{L,m_L}|^2 \tag{5}$$

where the kinematical factor C has the value $C = (2\pi)^4 p_a p_b / p_o$. The transition matrix elements $T_{L,mL}$ are given by

$$T_{L,m_L} = \langle f|(1 + V_f G)V_i(\epsilon_j \cdot \boldsymbol{r}_b)|i\rangle \tag{6}$$

In Eq. (6) ϵ_j refers to the polarization of the laser and $\boldsymbol{r}_b$ is the coordinate of the valence electron of *Na* with respect to the nucleus. The state vectors $|i\rangle$, $|f\rangle$ are asymptotic states of the projectile–atom system in the initial and final channel, respectively, and are determined as eigenfunctions of the asymptotic Hamiltonian h_i, h_f with appropriate boundary conditions. The perturbations V_i, V_f are then given by $V_{i/f} = H - h_{i/f}$. G is the resolvent of the total Hamiltonian H that is given by:

$$H = -\frac{1}{2}\nabla_{r_a}^2 - \frac{Z_{Na}}{r_a} + \frac{1}{|\boldsymbol{r}_a - \boldsymbol{r}_b|} + \sum_{j=1}^{Z_{Na}-1} \frac{1}{|\boldsymbol{r}_a - \boldsymbol{r}_j|} + H_{Na} \tag{7}$$

In Eq. (7) $\boldsymbol{r}_a$ stands for the position of the projectile with respect to the nucleus of *Na*, $Z_{Na} = 11$ is the nuclear charge, and $\boldsymbol{r}_j$, $j = 1...10$ are the coordinates of the core electrons of *Na*. For the description of the valence ground state of the undistorted sodium atom we assume the effective one-particle Hamiltonian:

$$H_{Na} = -\frac{1}{2}\nabla_{r_b} - V_{klap} \tag{8}$$

where the effective one-particle potential V_{klap} is given by [9,10]

$$V_{klap} = -\frac{1}{r_b} - \frac{Z_{Na} - 1}{r_b}\exp(-\alpha_1 r_b) - \alpha_3 \exp(-\alpha_2 r_b) \tag{9}$$

where $\alpha_1 = 7.902$, $\alpha_2 = 2.688$, and $\alpha_3 = 23.51$. If we choose h_i as $h_i = -1/2(\nabla_{r_a}^2 + \nabla_{r_b}^2) - 1/r_b$, we obtain for V_i

$$V_i = -\frac{Z-1}{r_b}\exp(-\alpha_1 r_b) - \alpha_3 \exp(-\alpha_2 r_b) - \frac{Z_{Na}}{r_a} + \frac{1}{|\boldsymbol{r}_a - \boldsymbol{r}_b|} + \sum_{j=1}^{Z_{Na}-1} \frac{1}{|\boldsymbol{r}_a - \boldsymbol{r}_j|} \tag{10}$$

Evaluation of scattering amplitudes with the initial-state scattering potential V_i that contains scattering

from all electrons of Na is intractable. Therefore we take only the monopole term (with respect to $r_a \gg 1$) of V_i, i.e., $V_i \approx \lim_{r_a \gg 1} V_i$. Obviously, this approximation is appropriate for large impact parameters.

The state vector $\langle \Psi| = \langle f|(1 + V_f G)$ is determined as an eigenstate of H with two-electron outgoing wave boundary conditions. Again, to reduce the many-electron Hamiltonian H to a three-body system we have to decouple the degrees of freedom of the two-continuum electrons from those of the sodium-core electrons. This is achieved by the (monopole) approximation $H_f \approx \lim_{r_a \gg 1, r_b \gg 1} H$. Clearly, this 'frozen core' approximation breaks down at low energies of the continuum electrons. The three-body eigenstate $|\Psi\rangle$ of H_f is approximated by a product of three two-body Coulomb waves with dynamical coupling between the individual two-body subsystems being included (hereafter DS3C) [11]

$$\langle r_a, r_b|\Psi\rangle \approx N e^{i\boldsymbol{p}_a \boldsymbol{r}_a} e^{i\boldsymbol{p}_b \boldsymbol{r}_b}\, {}_1F_1[i\beta_a, 1, -i(p_a r_a + \boldsymbol{p}_a \cdot \boldsymbol{r}_a)]$$
$$\times {}_1F_1[i\beta_b, 1, -i(p_b r_b + \boldsymbol{p}_b \cdot \boldsymbol{r}_b)]$$
$$\times {}_1F_1[i\beta_{ab}, 1, -i(p_{ab} r_{ab} + \boldsymbol{p}_{ab} \cdot \boldsymbol{r}_{ab})], \qquad (11)$$

where $\boldsymbol{r}_{ab} = \boldsymbol{r}_a - \boldsymbol{r}_b$ and $\boldsymbol{p}_{ab}$ its conjugate momentum. ${}_1F_1[a,b,c]$ is the confluent hypergeometric function and N is a normalization factor. The explicit form of the dynamical Sommerfeld parameters β_j, $j = a,b,ab$ has been given elsewhere elsewhere [12].

In the second calculation we remove the dynamical screening in the final continuum state of the two electrons and the ion. This is done by replacing the dynamical Sommerfeld parameters in [11] by the standard Sommerfeld parameters, in which the final two electron continuum state is represented by the correlated BBK wavefunction [13], which we call the 3C calculation.

The third calculation is the First Born Approximation (FBA), obtained from Eqs. (10) and (11) in the limit $\beta_a \equiv 0 \equiv \beta_{ab}$. Within the FBA and for hydrogenic targets Fehr the dichroism (3) possesses [5] the structure $\Lambda_0^{(1)} \propto \hat{e}_z(\boldsymbol{q} \times \boldsymbol{p}_b)$ with $\hat{\boldsymbol{e}}_z$ being the quantization axis of the target and $\boldsymbol{q} = \boldsymbol{p}_0 - \boldsymbol{p}_a$ is the momentum transfer, i.e. the angular dependence of $\Lambda_0^{(1)}(\hat{\boldsymbol{p}}_b)$ shows a reflection antisymmetry with respect to $\hat{q}$, and hence $\Lambda_0^{(1)}(\hat{\boldsymbol{p}}_b)$ vanishes at $\hat{\boldsymbol{p}}_b \| \hat{\boldsymbol{q}}$ (in the present work $\hat{\boldsymbol{e}}_z$ is perpendicular to the scattering plane spanned by $\hat{\boldsymbol{p}}_b, \hat{\boldsymbol{p}}_a$ *and* $\hat{\boldsymbol{p}}_0$).

4. Results

Two peaks are observed in the binding energy spectrum corresponding to ionization from the ground $3S_{1/2}$ and the excited $3P_{3/2}(m_L = \pm 1)$ states. From the sum of counts under each peak, for both positive and negative orbital orientations, the relative ionization cross-sections were determined. In Fig. 2, experimental angular correlations derived from a series of such spectra are presented. The incident beam energy was set to 150 eV, the detection angle for the fast outgoing electrons was 20° and the slow electrons were measured over an energy band of 20 ± 3 eV. The experimental results have been normalized to the $m_L = -1$ DS3C peak. As expected, the cross-section sections $\sigma_{0,0}$ for ionization from the $3S_{1/2}(F = 2, m_F = +2)$ and from the $3S_{1/2}(F = 2, m_F = -2)$ ground states are identical. In contrast, for the $3p$ excited states, the cross-section depends strongly on

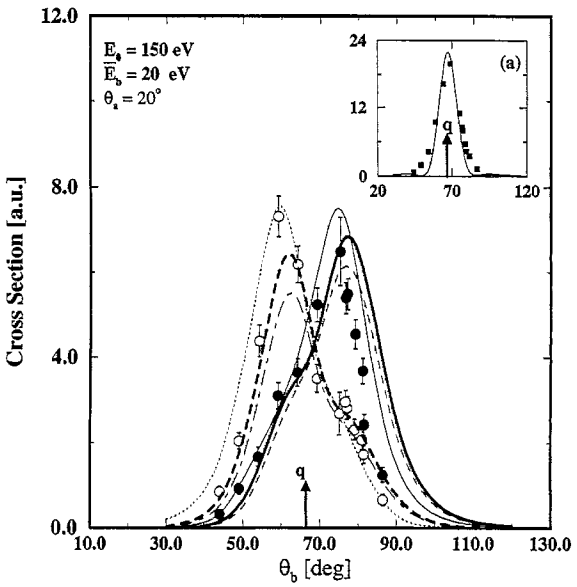

Fig. 2. The 150 eV (e,2e) cross-section on Na $3^2P_{3/2}$, $m_F = -3$ (filled circles) and $m_F = +3$ (open circles) for $\theta_a = 20°$, $\phi_a - \phi_b = \pi$ and $\bar{E}_b = 20$ eV. The corresponding FBA (scaled down by a factor of 2), 3C (multiplied by a factor of 1.4) and DS3C cross-sections are indicated, respectively by thin solid and dotted lines, thin dashed and dash–dotted lines, and thick solid and dashed lines. The measurements are normalized to the $m_L = -1$ DS3C cross-section peak. The momentum transfer direction is given by $\vec{q}$. The inset shows the ground state Na $3_2S_{1/2}$ transition normalized to the FBA cross-section.

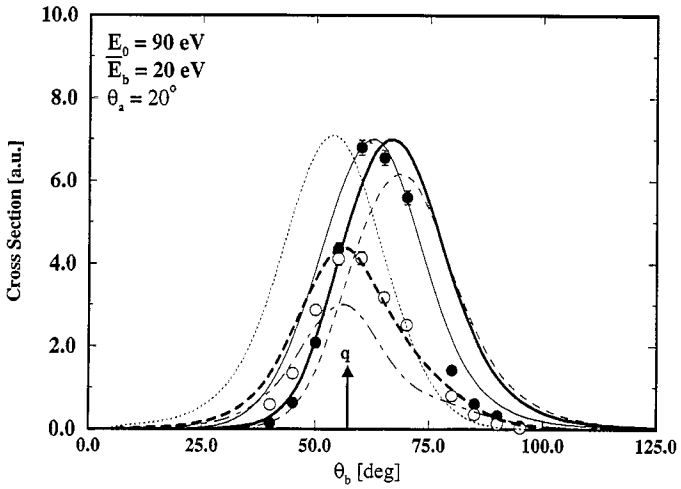

Fig. 3. As in Fig. 2 except for incident energy of 90 eV. Inset shows the ground state cross section normalized to the DS3C calculation (solid line).

the orbital angular momentum substate excited by the laser pumping process.

The transformation properties of $\Lambda_0^{(1)}$ within the framework of the FBA, i.e. the reflection symmetry between $\sigma_{1,\pm 1}$ about $\hat{q}$, are evident from the figure where the FBA calculation is seen to provide an adequate description of all cross-sections for these kinematics. As expected at an energy of 150 eV the DS3C calculation is quite close in shape to the FBA, although the DS3C cross-sections are moved to larger angles, primarily attributable to the effects of final-state electron correlation. The 3C calculation (multiplied by a factor of 1.4) has essentially the same shape as the DS3C results, showing an insensitivity to the details of the treatment of final state correlations under these particular kinematical conditions. The FBA calculations (multiplied by 0.5 in the figure) predict larger cross-sections than higher order theories. Inset (a) in Fig. 2 shows the $Na(3^2S_{1/2})$ cross-section, normalized to the FBA calculation. The cross-section is independent of laser polarization and symmetric with respect to $\hat{q}$, again agreeing quite well in shape with the FBA.

For the data shown in Fig. 3, the incident beam energy was lowered to 90 eV for the same fast electron scattering angle θ_a of 20° and slow electron energy band of 20 ± 3 eV. The experimental data has been normalized to the DS3C calculation of $\sigma_{1,-1}$ at 60°. Clearly the FBA cannot account for the behaviour of $\Lambda_0^{(1)}$ at this lower incident energy as there is no longer reflection symmetry between the measured $m_L = \pm 1$ cross-sections about the momentum transfer direction. The DS3C calculations describe the experimental data quite well in shape, the angular positions of the cross-section maxima and their relative magnitudes. The 3C calculation also predicts large dichroism effects, but does not fit the data as well as the DS3C calculation, demonstrating the utility of using the dynamical Sommerfeld parameters over the standard Sommerfeld parameters at lower energies. The shift of the measured cross-section from the FBA predictions can be largely traced to final-state electronic correlations that are included in both the DS3C and 3C models.

5. Concluding remarks

We have presented experimental results representing the first observation of orientational dichroism in the electron-impact ionization of an oriented target atom. The dependence of the cross-section on the orientation of the initial state is dynamically related to the phase of the final state wavefunction, which is a very sensitive quantity. At low energies, final state correlations are extremely important, significantly reducing the $m_L = +1$ cross-section relative to the $m_L = -1$ cross-section.

Acknowledgements

A.D. gratefully acknowledges support from the Deutsche Forschungsgemeinschaft and the Research School of Physical Sciences and Engineering at the Australian National University. J.B. acknowledges financial support by the Alexander von Humboldt Foundation and the Research School of Physical Sciences and Engineering.

References

[1] H. Ehrhardt, K. Jung, G. Knoth, P. Schlemmer, Z. Phys. D 1 (1986) 3.
[2] I.E. McCarthy and E. Weigold, Electron–Atom Collisions, Cambridge University Press, 1995.
[3] I.E. McCarthy, E. Weigold, Rep. Prog. Phys. 54 (1991) 789.
[4] E. Weigold, Y.Q. Cai, S.A. Canney, A.S. Kheifets, I.E. McCarthy, P. Storer, M. Vos, Aust. J. Phys. 49 (1996) 543.
[5] M. Fehr, J. Berakdar, H. Klar, J. Phys. B 27 (1995) L401.
[6] B. Granitza, X. Guo, J.M. Hurn, J. Lower, S. Mazevet, I.E. McCarthy, Y. Shen, E. Weigold, Aust. J. Phys. 49 (1996) 383.
[7] E.E.B. Campbell, H. Hülser, R. Witte, I.V. Hertel, J. Phys.D: Appl. Phys. 16 (1990) 21.
[8] J. Berakdar, A. Engelns, H. Klar, J. Phys. B 29 (1996) 1109.
[9] M. Klapisch, PhD Thesis, University of Paris-Sud Orsay, 1969.
[10] C. Courbin, M. Machholm, E. Lewartowski, Z. Phys. D. 30 (1994) 205.
[11] J. Berakdar, Phys. Rev. A. 53 (1996) 2314.
[12] J. Berakdar, J. Röder, J.S. Briggs, H. Ehrhardt, J. Phys. B 29 (1996) 1767.
[13] M. Brauner, J. Briggs, H. Klar, J. Phys. B 22 (1989) 2265.